
REALIZING FLAME STATE MONITORING WITH VERY FEW VISUAL OR INFRARED IMAGES VIA FEW-SHOT LEARNING

Ruiyuan Kang

Department of Mechanical Engineering
Khalifa University
Abu Dhabi, UAE
ruiyuan.kang@ku.ac.ae

Panos Liatsis

Department of Electrical Engineering and Computer Science
Khalifa University
Abu Dhabi, UAE
panos.liatsis@ku.ac.ae

Dimitrios C. Kyritsis

Department of Mechanical Engineering
Research and Innovation Center on CO₂ and Hydrogen
Khalifa University
Abu Dhabi, UAE
dimitrios.kyritsis@ku.ac.ae

ABSTRACT

Machine learning/ deep learning has been proved to be capable to realize image-based combustion monitoring. However, the success of these algorithms is based on massive data, which is costly even impossible for industrial applications. To address this conflict, we introduce few-shot learning to combustion monitoring field for the first time. Two algorithms are attempted here, they are Siamese Network coupled with k Nearest Neighbors (SN-kNN) and Prototypical Network (PN), respectively. Besides, rather than purely utilizing visual images as previous studies, we also attempt Infrared (IR) images, since many fuels, combustion products have strong signals in Infrared wavelength. In this work, we analyze the training process, test performance and inference speed of these two algorithms on both two image formats, and also use t-SNE algorithm to visualize learned features. The results demonstrate that both SN-kNN and PN are capable to distinguish flame states from learning with 20 images per flame state. The worst performance, which is realized by combination of PN and IR images, still possesses precision, accuracy, recall, and F1-score all above 0.95. Through observing images and visualizing features, we realize that visual images have more dramatic differences between classes and have more consistent patterns inside the class, which makes the training speed and model performance on visual images is better. In contrast, the relatively "low-quality" IR images makes PN hard to extract distinguishable prototypes, which causes the relative weak performance, but with the whole training set to support classification, SN-kNN cooperates well with IR images. On the other hand, benefited from the architecture design, PN has a much faster speed in training and inference than SN-kNN. The work here analyzes the characteristics of both algorithms and image formats for the first time, which provides the guidance for further utilizing them in combustion monitoring tasks.

Keywords Combustion state monitoring · Few-shot learning · Visual images · Infrared images

1 Introduction

Combustion is one of the most fundamental phenomena of nature and one of the dominating ways that human utilizes the energy. Meanwhile, it is an intense chemical process with complex hydrodynamics. Therefore, in order to assure the safety, quality, controllability, and recently popular, environmental friendliness of combustion, combustion monitoring is mandatory in utilizing combustion phenomenon.

Table 1: Brief categories of work on AI-assisted image-based combustion state monitoring

Technology route	Authors
Handcrafted features + classical supervised learning	Zhou H, et al. [4], Bai X, et al. [3], Pino J, et al. [6], Wang Y, et al. [7], Chen H, et al. [8], De Santana, et al. [9], Li W, et al. [10], Hauser M, et al. [11], Chui DS, et al. [12], Chen J, et al. [13, 14], Sun D, et al. [15]
Representation learning + classical supervised learning	Wang Y, et al. [7], Han Z, et al. [5, 16], Akintayo A, et al. [17], Qiu T, et al. [18]
Deep supervised learning	Wang Z, et al. [19], Zhu X, et al. [20], Li T, et al. [21], Choi O, et al. [22]

Although popular laser-based diagnostics [1] has achieved tremendous success in the field of combustion monitoring, passive optical gas image [2] is gradually attracting attentions in the terms of being a potential combustion monitoring tool. Because using a portable camera rather than a laser-based system is more convenient, general and lower costly. Nevertheless, the information delivered by optical images is implicit and elusive for ordinary people, although some experienced engineers may have the sense to approximately infer flame images.

Recently, the burgeon of AI has been gradually alleviating the dependencies on engineers and enabling various combustion monitoring tasks, e.g., monitoring combustion instability [3], classifying combustion composition [4, 5], classifying combustion propensity [6], etc. In general, the methodologies utilized in these studies can be divided into three routines (Table 1), they are respectively (1) coupling handcrafted features with classical supervised learning; (2) coupling representation learning with classical supervised learning; (3) Deep Supervised learning.

In fact, the first and second categories have similar ideas that extracting low dimensional features to represent high dimensional images, thus, to avoid the dimensionality curse may happen in classical supervised learning process. But, in concrete implementations, these two categories of methods have intrinsic difference.

For the first category, the features are extracted by multiple processes explored and designed by researchers themselves through their domain knowledge. For example, Ref. [13, 14] utilized Principal Component Analysis (PCA) [23] to compress the images into low dimensional vectors, i.e., features, based on that, Ref. [3, 15] used upgraded kernel PCA [24], which can further extract nonlinear features to describe images. Besides, Ref. [7, 8] chose to use statistical parameters, such as norms and Kurtosis, to describe images. In addition, the operations of image processing were often referred to do the work, such as utilizing Gabor filter [10], histogram of oriented gradients [11], and Ibrahim time-domain transform [12], etc.

However, such an manual feature engineering is time-consuming since massive combinations need to be explored in order to find a proper way to describe images. To tackle this shortcoming, in second category, the features are extracted automatically through machine learning algorithms. For example, Wang Y. et al. [7] utilized self-organization map [25], a competitive learning algorithm, to learn low dimensional features, Ref. [5, 17, 18] utilized diverse versions of auto encoder to embed images [26] into compact features; Hossain, et al. [16] utilized Generative Adversarial Network(GAN) [27] to learn more robust features in an adversarial way. Once informational features are extracted, both categories have no difference in utilizing classical supervised learning algorithms to realize combustion monitoring, i.e., mapping features to diverse classes, such as combustion states. The classical supervised learning algorithms have been attempted include Support Vector Machine (SVM) [28], Multi-Layer Perceptron(MLP) [29], Gaussian process [30], etc.

The third category encapsulates the feature engineering and classification into an integral process, what is termed as end-to-end learning. Therefore, the features learned are classification oriented, which is more targeted. In general, this idea is realized by convolution neural networks [31], and some other works [21, 22] also coupled recurrent neural network [32] to utilize the temporal information from image sequences.

In any ways, these works contribute significantly to the development of image-based combustion monitoring. But, the fact of the matter is that a tremendous amount of data, at least thousands of images, are needed for training a machine learning model, especially, a deep learning one. This correspondingly represents that (1) massive time and resource will be costed inevitably, on the purpose of collecting, organizing and labelling images; (2), To utilize the massive data, massive time and computation resources are needed to train a convergent model, i.e, which is expensive in either time or cost. However, these two requirements conflict with industrial application conditions that (1) industrial applications of combustion monitoring cannot provide sufficient effective data in most cases, since abnormal/unwanted state is avoided deliberately in industrial operation, and many of them are transient process, so that very few images of them can be captured. (2) Industrial applications are not willing to wait for a long time to collect data and train models before deployment, instead, they want these technologies to work as soon as possible. Therefore, to alleviate the conflicts, an intelligent system which can learn efficiently from very limited data is needed.

In addition to the consideration of algorithm, To authors' best knowledge, the registered publications only work with images in visual bands. However, we realized IR images may be also a potential alternative, since many interested

fuel and products of combustion have strong signals in IR bands, such as hydrocarbons, Ammonia, CO_2 , CO , and NO_x . Meanwhile, the most atmosphere gases such as Nitrogen and Oxygen are transparent in IR bands, so which will not disturb the signal. Therefore, it is also theoretically feasible and competitive to utilize Infrared (IR) images for combustion monitoring.

According to the discussion above, we propose two few-shot-learning based combustion monitoring algorithms, in which, Siamese Network with k nearest Neighbors, and Prototypical Network, are respectively utilized to realize combustion state classification task. Rather than singly training and testing these algorithms on visual images, we also assess the feasibility of utilizing IR images. The contributions of this work are summarized as follows.

1. We introduced few-shot learning into the field of combustion monitoring for the first time, which can significantly save the data needed for training a deep learning model, and thus massively reduce the time needed for training.
2. We assessed and proved the feasibility of utilizing IR images to realize combustion monitoring task for the first time.
3. We compared the performance and analyzed the characteristics of both algorithms on both image formats, which provides the reference for further utilizing these algorithms.

2 Methodology

2.1 Experiment setup and data acquisition

First, we need to acquire IR and visual images of flames at different states. In order to do so, we executed combustion experiments on the counterflow burner built in Khalifa University [33]. Fig. 1 shows the configuration of the burner, which is composed of two nozzles in general. O_2 and CH_4 are respectively pumped to the upper and lower nozzle, H_2O is supplied to the upper nozzle for cooling. In addition, N_2 is pumped to both nozzles optionally to stabilize the flame. We used two cameras to observe the flames. One is FASTEC TS-5 high-speed CMOS camera, its detectable wavelength range is 350-950 nm, so used to capture visual images. The other is FLIR E95 IR camera, whose detectable wavelength range is 7-15 μm .

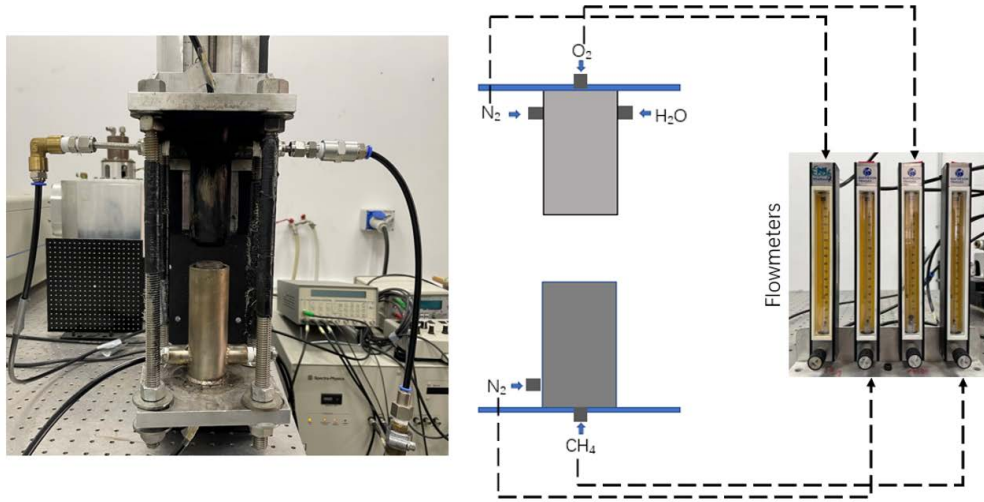


Figure 1: The burner and schematic of gas links

In experiments, six different reactant conditions are set, the flames consequently generated are regarded as six combustion states, which are also termed as classes in machine learning. Matheson rotameters measured the nitrogen, oxygen, and methane gases at every state. The rotameters provided volume flow rate measurements with an estimated error of 5% according to the specifications of the manufacturer. The scale readings were converted to mass flow rates, as shown in Table 2.1.

We used two cameras alternately to take images of flames. The Frame Per Second (FPS) is 100 and 30 for CMOS and IR camera, respectively. Each camera was used for about 20 seconds to take images of a given state (class). Examples of visual images and IR images are respectively displayed in Fig. 2 and Fig. 3.

Table 2: Setting of Reactant ratios

Reactants (g/s)	N_2 to O_2	N_2 to CH_4	O_2	CH_4
Class 1	1.03	0.52	1.82	0.77
Class 2	1.14	0	2.01	1.19
Class 3	2.72	0	2.68	0.92
Class 4	0	0	0.95	0.52
Class 5	2.02	1.19	1.25	0.78
Class 6	1.11	1.04	1.28	1.25

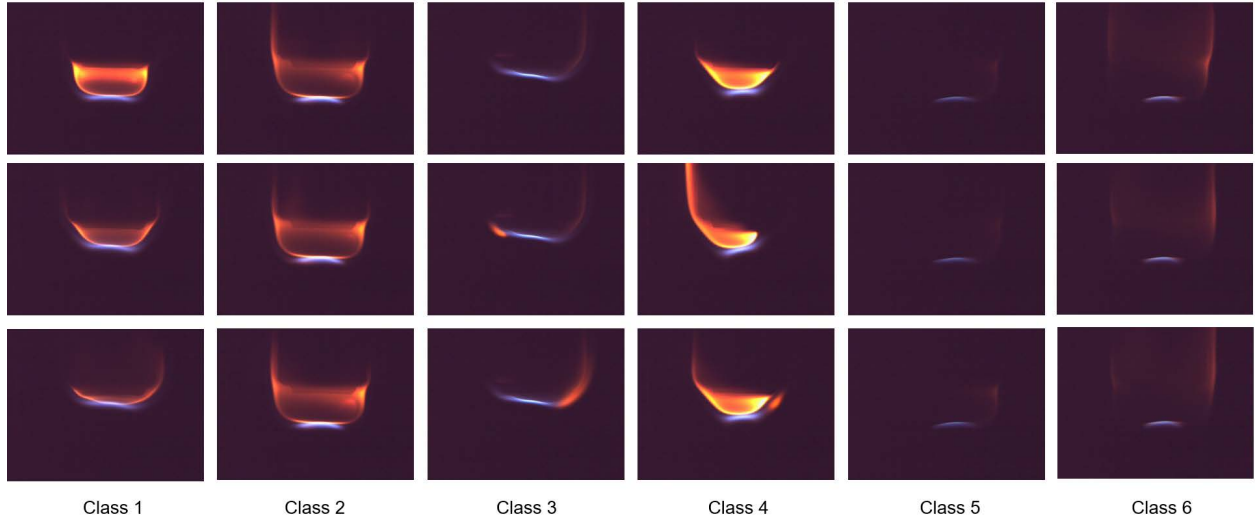


Figure 2: Visual images of six flame states

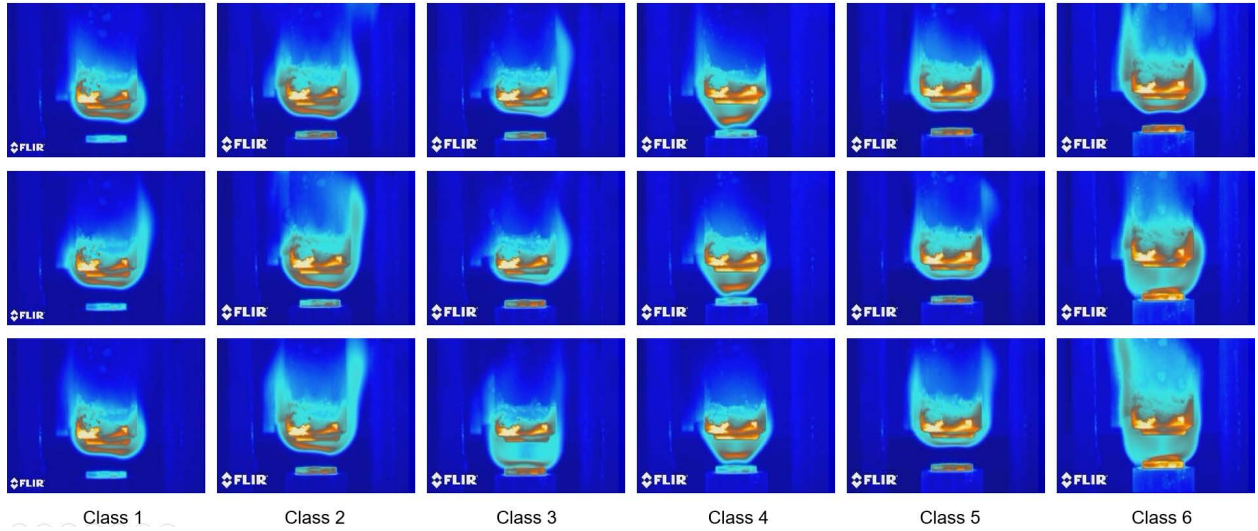


Figure 3: IR images of six flame states

After image collection, twenty images were randomly picked from every state to construct a training set, and another twenty images were used to build a validation set. To thoroughly evaluate the performance of few-shot learning models, a much larger test set, contains 400 images per state, was built. It is notable that only images in training set, i.e., 20

images per state, are used to tune the learnable parameters in models. As one can see, it is a much less image amount compared to what have been reported (Table 1).

2.2 Few-shot learning algorithms

In this work, two few-shot learning algorithms were explored, one is Siamese Network (SN) [34], which is initially designed to distinguish the similarity of two images, so in order to realize the flame state classification purpose, we couple it with K Nearest Neighbors (KNN) algorithm [35]; the second algorithm is Prototypical Network (PN) [36]. In following sections, we briefly introduced the their specific design for the flame state classification task herein.

2.2.1 Siamese Network coupled with k Nearest Neighbors (SN-kNN)

Siamese network is a contrastive-learning-style few-shot learning algorithm. The function of SN herein is to learn compact encoding of samples which elaborate the class differences between two image samples. To do so, we first label pairs of images from the same class with the value of one, and label pairs of images from different classes as zero, (Eq. 1,

$$label = \begin{cases} 0 & s_i, s_j \in class_c \\ 1 & s_i \in class_c, s_j \notin class_c \end{cases} \quad (1)$$

where, s represents the image sample, the subscripts i, j, c respectively represent the sample indexes of two image samples, and a state/class index.

Then image pairs were fed to SN, the SN outputs a single value in the range of [0,1] for every pair to imitate the corresponding label of the image pair. The SN architecture utilized is demonstrated in Fig. 4. It can be mainly divided into two parts, encoding module and prediction module. The encoding module contains two parallel encoding layers, which is used to extract features from images. Herein, we utilized the convolution layers of VGG13 [37] to be encoding layers, of course, any other convolution layers [38], even attention layers [39] can realize the same function. The two VGG13 used here share the same weights, i.e., they are identical in the terms of architecture and values of learnable parameters. After encoding the two images into two compact features, either of them has a dimension of 2048, the absolute differences of these two features in every entry are fed to the prediction module. The prediction module contains two projection layers (dense layers), which helps map the differences into a single value, and then a Tansig function was used compress the output into the range of 0-1, for the purpose of mimicking labels. The learnable parameters of SN are updated by the binary cross entropy loss defined by the ground truth and prediction of labels.

As aforementioned, the SN only indicates whether two images belong to the same classes or not, therefore, we added k nearest neighbors (kNN) to complement the classification function. The general idea of kNN is that, for a class-unknown test sample, it should have the same class belongingness as its most similar samples. Taking this idea in mind, we utilized KNN in the way shown in Fig. 5. To check the class of one unseen test sample, the test sample is paired with every sample in the training set, and then be fed to SN, the corresponding prediction from the SN indicate the level of similarity between the test sample and a specific training sample. Therefore, we can pick the training samples reaching the first k minimal values of predictions to construct a decision set, and then use the class belongingness of most samples in decision set as the class of the test sample. To avoid the ambiguity caused by potentially balanced vote between training samples, the k value used should be an odd number, which is 5 herein.

2.2.2 Prototypical Network

Very different from SN, PN realizes the function of classification directly by utilizing the concept of prototype. Training of PN can be also divided into two parts, as shown in Fig. 6. The first part, constructing prototypes. Randomly picking n samples per class to construct a support set, then encoding these samples of support set into vector-style compact features by a encoding module, which is again VGG13 herein, and then averaging the features within the same class to acquire the prototype of the corresponding class (Eq. 2),

$$v_{pt,c} = \frac{\sum_{i=1}^n v_i}{n} \quad i \in class_c \quad (2)$$

Where, v is the encoded features. The subscript pt represents the prototype. As we can see, the prototype is the center of the feature distribution per class, thus, can be regarded as the most comprehensive representative of the given class.

The second part, updating PN. Generating a query set by picking samples per class from the training set aside of the support samples. Again, the features of these query samples were also encoded by the encoding module used above. After that, we calculated the Euclidean distances between the features of query samples and all prototypes.

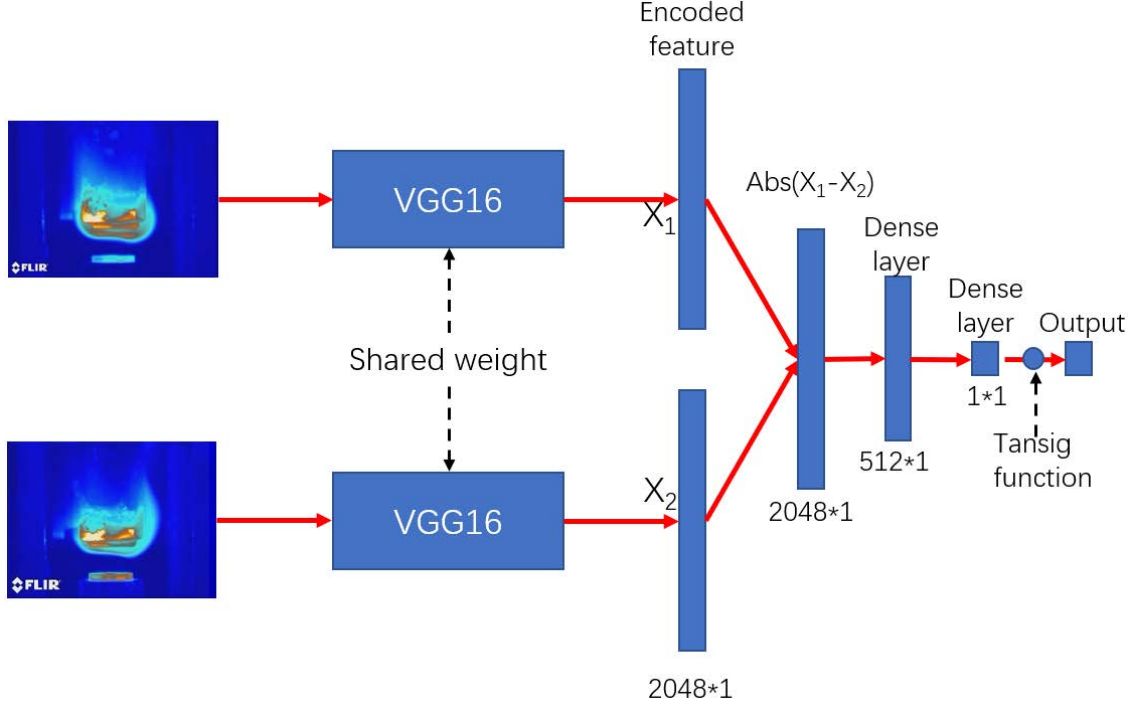


Figure 4: The schematic of architecture of Siamese Network

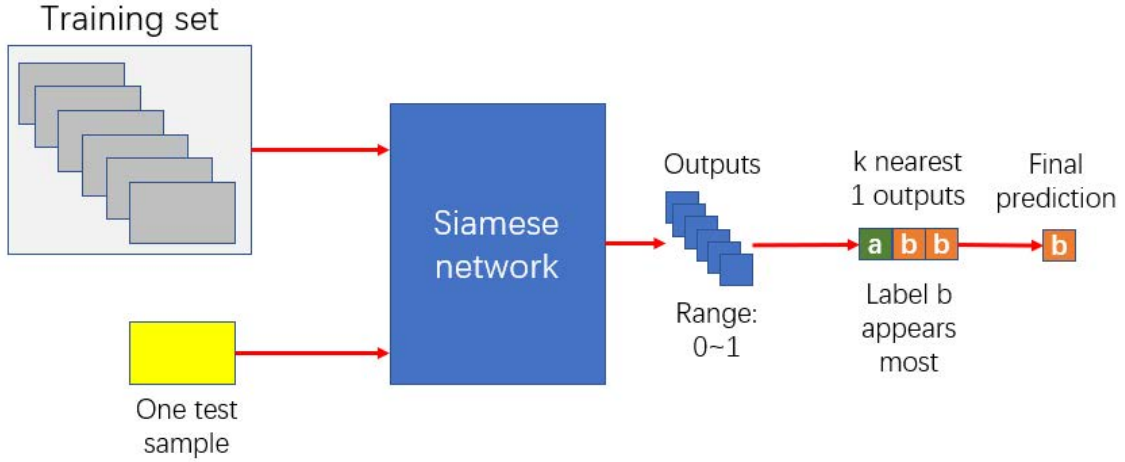


Figure 5: The schematic of integral flowchart of SN-kNN

The distances are transformed to the possibility of the query sample belongs to the specific class by utilizing SoftMax function ,i.e., Eqs. 3 4.

$$d_{i,c} = \|v_i - v_{pt,c}\|_2 \quad (3)$$

$$P_{i,gc} = \frac{\exp(-d_{i,gc})}{\sum_{c=1}^m \exp(-d_{i,c})} \quad (4)$$

Where, d, P are respectively distance and probability. The subscripts gc, m respectively demonstrate the given class and total class number. Therefore, the closer between a query sample and a prototype of given class, the higher $P_{i,gc}$ is,

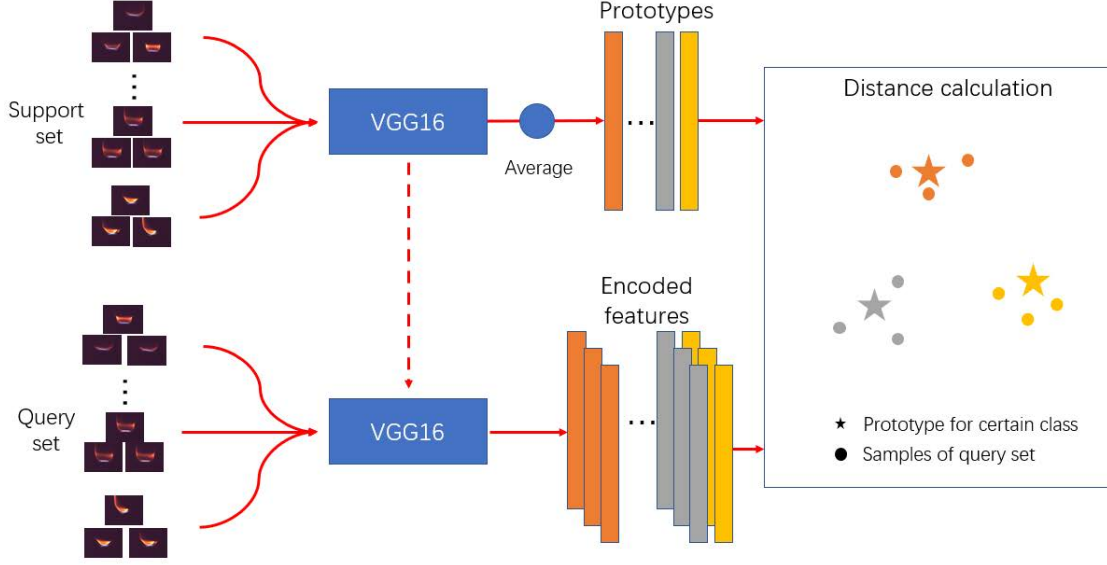


Figure 6: The schematic of architecture of Prototypical Network

vice versa. Since the ideal case we would like to reach is that the query sample is closest to the prototype of its own class instead of those of other classes, thus, the loss for updating PN can be defined by Cross Entropy Loss (CELoss) function (Eqs. 5, 6):

$$L = \frac{1}{N} \sum_{i=1}^N \sum_{gc=1}^M - [y_{i,gc} \log(P_{i,gc}) + (1 - y_{i,gc}) \log(1 - P_{i,gc})] \quad (5)$$

$$y_{i,gc} = \begin{cases} 1 & s_i \in gc \\ 0 & s_i \notin gc \end{cases} \quad (6)$$

Where, L , N , y are respectively the loss function, total sample number of whole query set, the class indicator of a given sample. As one can see, by minimizing this loss function through updating the encoding module, the encoding module will modify the way of embedding images, and tend to make all samples from the same class cluster around the prototype of the class, and extend the distance between samples and prototypes from different classes.

2.2.3 Training method

Classical epoch-batch training method was used to train SN. In every batch, 15 images were randomly sampled from the training set. For every image picked, two other images were also picked from the same and a different classes respectively, i.e., positive sample and negative sample for the current sample. Consequently, 15 positive samples plus 15 negative samples make up 30 image pairs with original sampled images. For convenience, we arbitrarily set one training epoch contains four batches of training. The value four is the quotient of the total number of samples in the training set and the amount of sample pair in each batch.

Episodic training method was used to train PN. The episodic training is also constituted by multiple epochs, and every epoch is made up by multiple episodes. The term episode is the counterpart concept of batch, but training of every episode is executed by support set and query set of training set rather than directly the training set. In the training of one episode, we randomly picked five samples per class from the original training set as a support set and did that again from the remaining training samples to construct a query set. Hence, both the training-support set and training-query set had 30 samples. Similar to SN, we also set the number of episodes is four for one epoch training in order to further compare SN and PN in a pretty fair way.

The validation set was also processed in the same way we processed the training set for each algorithm. Once the accuracy on the validation set was improved, the model was automatically saved.

3 Results and analysis

3.1 Image transformation

In practice, the distance and relative location between the camera and the burner cannot be guaranteed to be identically same. To avoid models learning the fake features, such as the absolute size of flame or burner, flame location in the image, etc., we trained the model by utilizing image variants acquired from a series of deliberately designed image transformations. Moreover, image transformation is also a kind of data augmentation mean, so that helping avoid model overfitting on the small training set.

The detailed image transformation procedures are shown in Fig. 7. Step 1, center crop. For the processing convenience of network, the image was cropped to a square with the size of width of original image. Step 2, random scale. The image is randomly changed to the size of 1.1-1.5 times of the default input size for network (84*84). By doing so, the absolute size of flame from the same class is changeable, and thus will not be regarded as a pattern by models. Step3, random crop. The image was randomly cropped to the shape of 84*84, therefore, avoiding the position of flame to be learned as a feature. Step 4, horizontal flip. The image was randomly flipped with the possibility of 0.5 to simulate the case that flame image is captured from either of two opposite sides of the burner.

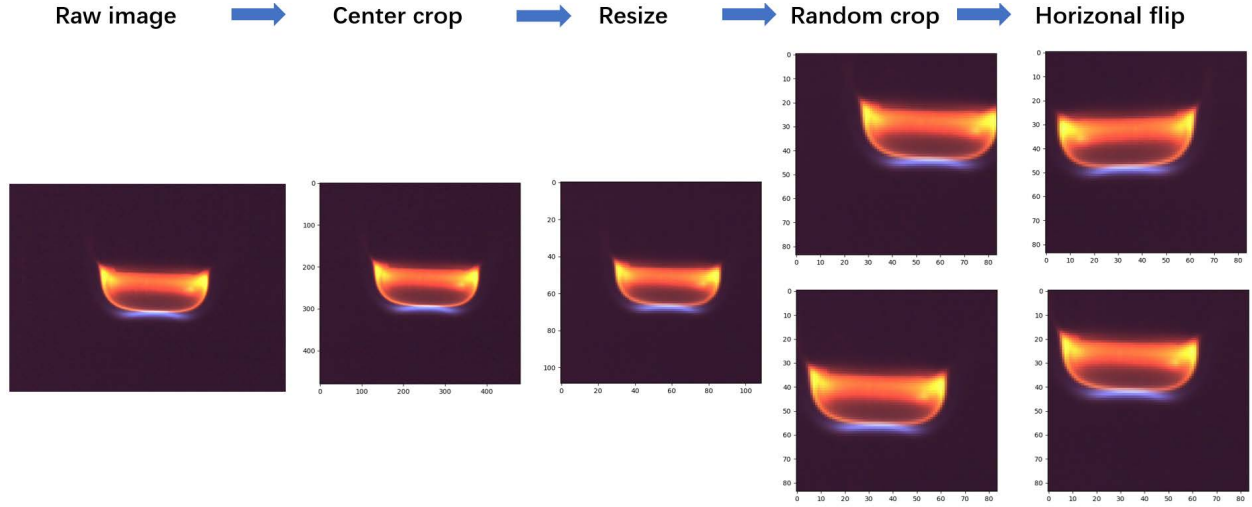


Figure 7: The schematic of procedure of Image transformation

3.2 Model training

The training and validation accuracy of two algorithms on two image formats in training process is shown in Fig. 8. Comparing the convergence time needed for both models, SN needs about 100 epochs to reach the accuracy of 1 (Fig. 8 (a) (b)). whereas PN only needs about 20-30 epochs training (Fig. 8 (c) (d)). The shorter model preparation time of PN is advantageous in industrial applications.

When looking at the training process on each data format, although SN needs similar amount of iterations to converge for both image formats, we can sense that the accuracy curve on visual images is flatter (Fig. 8 (b)), which presents a simpler training process. As for PN, this trend is even more apparent when comparing Fig. 8 (c) to Fig. 8 (d). Meanwhile, training on visual images is easier to get consistent training and validation accuracy (Fig. 8 (d)). In contrast, training on IR images has more fluctuation after reaching a prediction accuracy of 1 (Fig. 8 (c)). The observations above imply that visual image is more beneficial for the optimization of two models. The reason behind can be inferred intuitively from comparing visual images and IR images (Fig. 2, Fig. 3). When looking at visual images (Fig. 2), one can distinguish flames of different classes, since clear differences exist between classes and the flame appearances are consistent for the samples from the same class. However, IR images have much more color and texture information, and the differences between some classes are not clear enough for humans to make a reasonable classification. For example, some samples of class 1, class 2, class 3, and class 5 in Fig. 3 look similar. To some extent, the IR image has a worse quality than visual image regarding on the task issued herein, which makes models learn harder.

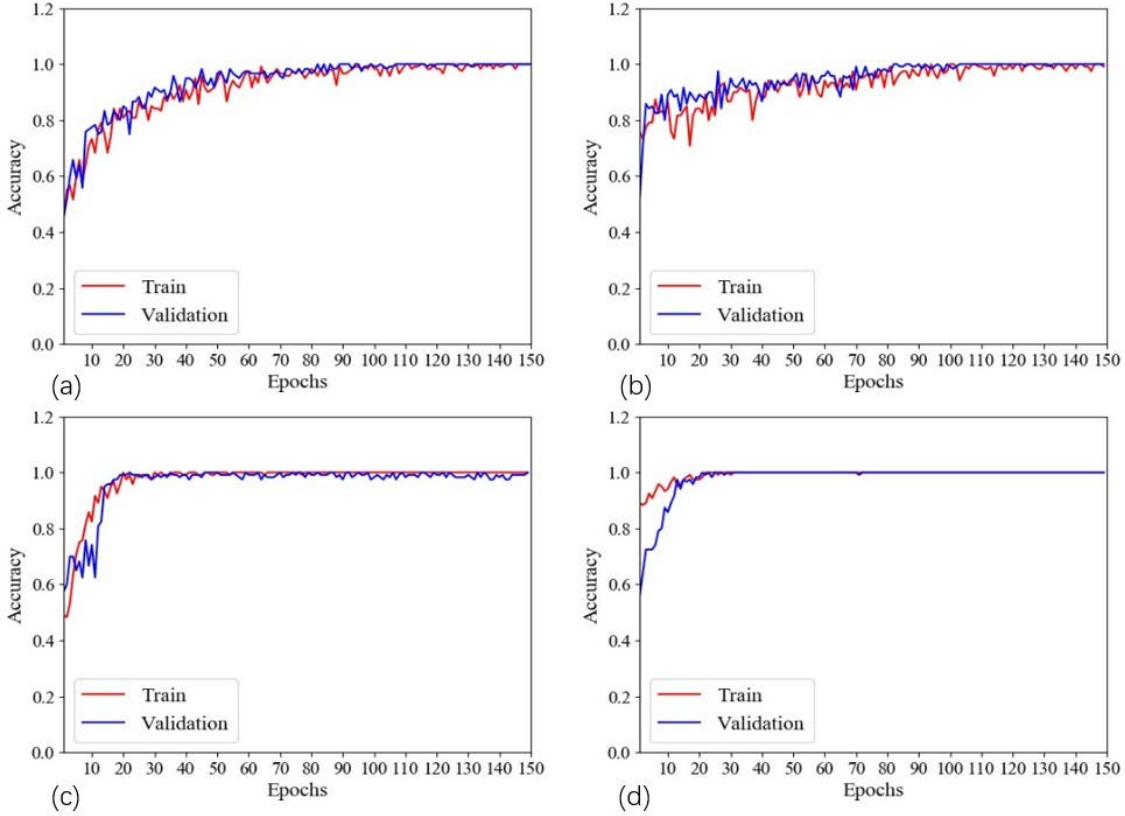


Figure 8: Training process of models. (a) SN on IR images (b) SN on visual images (c) PN on IR images (d) PN on visual images

3.3 Model testing

3.3.1 Prediction performance

We calculated the Precision, Accuracy, Recall, and F1-score for all models. The definitions of these four metrics are illustrated in Eqs. 7- 10.

$$A_c = \frac{TP_c + TN_c}{TP_c + TN_c + FP_c + FN_c} \quad (7)$$

$$P_c = \frac{TP_c}{TP_c + FP_c} \quad (8)$$

$$R_c = \frac{TP_c}{TP_c + FN_c} \quad (9)$$

$$F1_c = \frac{2 * P_c * R_c}{P_c + R_c} \quad (10)$$

In which, A_c , P_c , R_c , $F1_c$ means the Accuracy, Precision, Recall, and F1-score for particular class c , respectively. For particular class c , we can categorize the sample that belongs to this class as a positive sample; otherwise, the sample is regarded as a negative sample. TP i.e., True Positive, means the amount of correctly classified positive samples. TN i.e., True Negative, means the amount of correctly classified negative samples. FP , i.e., False Positive, means the amount of negative samples misclassified as positive samples. FN , i.e., False Negative, means the amount of positive samples misclassified as negative samples. To compare the model test performance comprehensively, we used the Macro-average method, i.e., using the average of the metric for every class as the final metric.

Table 3 summarized metrics of all models. As for the impact of algorithm, PN works worse on IR images, but this performance is still decent, with Precision equaling to 0.957, Accuracy, Recall, and F1-score about 0.953. Besides, PN

Table 3: Test performance of models

Algorithm	Data format	Precision	Accuracy	Recall	F1-score
PN	IR images	0.9570	0.9529	0.9529	0.9528
	Visual images	0.9975	0.9975	0.9975	0.9975
SN-kNN	IR images	0.9983	0.9983	0.9983	0.9983
	Visual images	0.9975	0.9975	0.9975	0.9975

and SN-kNN have equivalent performances on visual images. When it comes to the impact of image format, IR images obviously depressed the performance of PN. However, it does not disturb the performance of SN-kNN, in contrast, SN-kNN even has a slight advantage on IR images. Because only a few samples were misclassified for every model, the difference of various metrics cannot be highlighted, all of them have consistent values for a specific model.

More performance details are revealed in confusion matrix (Fig. 9). The confusion matrix provides the information about the classification distribution for a given class. For example, the first row of Fig. 9 (a) tells that except one image of class 1 was misclassified to class 2, SN-kNN correctly classified all the other 399 samples.

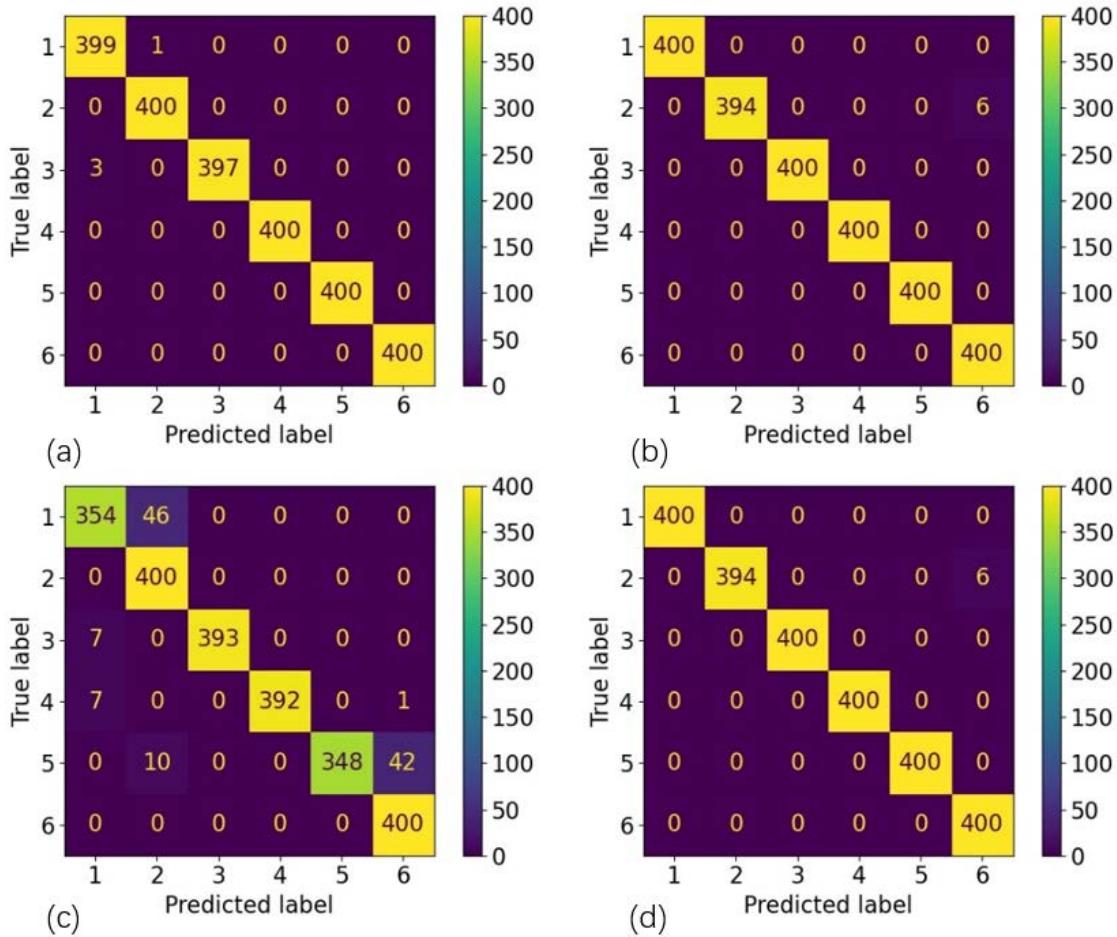


Figure 9: Confusion matrix of four models. (a) SN on IR images (b) SN on visual images (c) PN on IR images (d) PN on visual images

In general, except for the combination of PN and IR images (Fig. 9 (c)), all the other combinations work well. As for the case of PN working on IR images, about 11.5% samples of class 1 and 10% samples of class 5 were misclassified to class 2 and class 6, respectively. Fig. 10 displays some misclassified samples and typical images from the original classes and misclassified classes, it tells that the misclassified images from class 1 and class 5 are visually similar to the typical images of class 2 and class 6, so it is reasonable for misclassification happens. As for SN-kNN, it performs almost perfect on IR image (Fig. 9 (a)), although very few samples from class 1 and class 3 were misclassified.

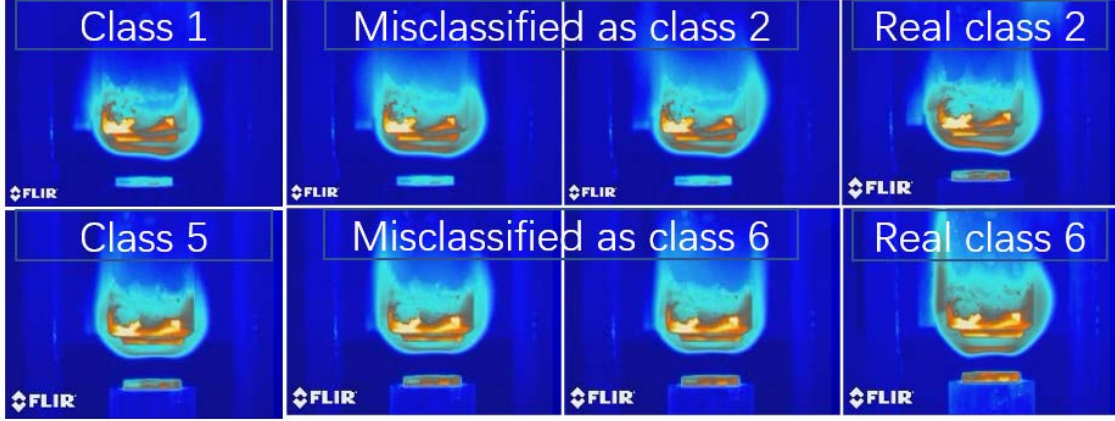


Figure 10: The IR images misclassified by PN and the typical images from correct and misclassified classes

As for the performance on visual images(Fig. 9 (b), (d)), both models misclassified the same six images of class 2 to class 6. Fig. 11 displays the two misclassified samples and typical images of class 2 and class 6. As one can see, the typical image of class 2 has an unbroken flame structure. However, these misclassified visual images are visually broken on the right side of the flame, which makes them more like the typical image of class 6 after horizontal flipping operation. Unfortunately, this horizontal flipping is indeed the transformation utilized herein. In addition, these six misclassified images were consecutively captured in experiments and was coincidentally not sampled by training set. To some extent, these six images can be regarded as outliers of the training set distribution, and consequently cause the confusion of models in test process. Thereby, it is notable that although few-shot learning algorithms can realize training of deep learning network with little data, it cannot learn the information that training images do not convey, as what happens to any other supervised learning algorithm.

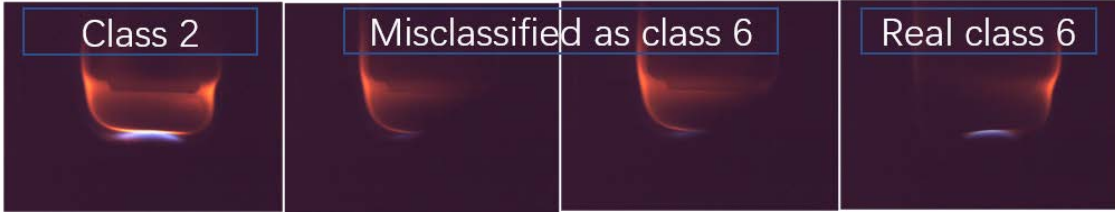


Figure 11: The visual images misclassified by PN and the typical images from correct and misclassified classes

Leaving these six outliers, both SN-kNN and PN work perfectly on visual images, but both models do have more classes been misclassified on IR band. This embodies that IR image seems less suitable for the task issued here, which is consistent to the discussion in training part.

Consequently, the lower quality of IR image harmed the performance of PN, although this did not happen to SN-kNN. The distinguishable performance difference between SN-kNN and PN is contributed by the reaction between mechanisms of algorithms and the characteristics of IR images. As for PN, it needs to summarize the characteristics of samples to construct representatives, i.e., prototypes. However, since IR images have more colorful patterns inside the class, it will be challenging for PN to generate the prototypes that can well represent the characteristics of their own classes. Meanwhile, the similar appearances of flame from different classes makes this task even harder. Luckily, for SN, there is no need to summarize the information to generate prototypes, instead, it tries to contrast the detailed difference between similar samples from different classes. Meanwhile, kNN does not care about the global distributions of whole class, instead, the local distribution around the test sample is more important. The contrastive learning style and decentralized mechanism makes SN-kNN more robust than PN.

3.3.2 Model inference speed assessment

Model inference speed is one vital metric needs to be considered for industrial applications, which is thereby assessed here. To simulate the actual combustion monitoring scenario, we fed the images in the validation set to models in a random sequence frame by frame. The test was executed in an ordinary laptop, whose GPU is GTX1650Ti, CPU is

Table 4: Inferece speed test results

Algorithm	Data format	Total proceession time for 120 images (ms)	Proceession time per frame (ms)	FPS
PN	IR images	5687.5	47.40	21.10
	Visual images	13984.38	116.54	8.58
SN-kNN	IR images	163046.88	1358.72	0.74
	Visual images	276250.00	2302.08	0.43

Intel Core i7-9750H. Table 3.3.2 shows the total inference time for 120 images, corresponding inference time per frame, and Frame Per Second (FPS).

Table 3.3.2 tells that PN needs 47.40 ms and 116.54 ms to classify one IR image or one visual image, respectively, while SN-kNN needs much more time, which is respectively about 28.66 times or 19.75 times than PN. This vast difference is mainly caused by algorithm structure. In the test process, the whole training set were used by SN-kNN, which is 120 images in total. However, only six prototypes were needed for PN. Moreover, the prototypes can be recorded in advance, therefore, PN only needs to encode test sample, but the temporal structure of SN asks all training samples go through the encoding for every test. In addition to the difference between algorithms, both few-shot learning algorithms need more time to process visual images than processing IR images, which is mainly due to more reading and transformation time is needed for processing visual image as it has a larger original size.

3.4 Feature visualization

In order to better understand the characteristics of image formats and algorithms, we used t-Distributed Stochastic Neighbor Embedding (t-SNE) algorithm [48], a dimensionality reduction algorithm, to map high dimensional features encoded by encoding modules to 2D features. The generated 2D features can be thus plotted for human to understand visually. T-SNE is an unsupervised algorithm, which means no label information is needed during feature mapping, it has the advantage of maintaining the relative distance relationship between features after dimensionality reduction, thus allowing to visually observe structure of dataset distribution.

The visualization results of 2D features generated by t-SNE are displayed in Fig. 12. As we can see, no matter for visual or IR images, the feature distributions within a specific class are similar for both SN and PN (Fig. 12 (a)(c) for IR images or (b)(d) for visual images). For example, irrespectively for SN or PN, the IR images of class 1 are encoded into three clusters, and a cluster of which can be further divided into two sub-clusters. This phenomenon elaborates that both algorithms learn the similar way to encode the samples inside the same class. However, SN and PN have different ways in coordinating relative positions between classes, e.g, the small cluster belongs to class 5 is encoded in a position close to class 3 by SN (Fig. 12 (a)), whereas, the same small cluster is guided to the position neighbors class 6 by PN (Fig. 12 (c)), which in turn leads to the misclassification of this small cluster.

Meanwhile, it can be observed that IR images have more clusters inside the class than visual images. For IR images (Fig. 12 (a)(c)), class 1 has three clusters, and class 3, 5, and 6 have two clusters; while for visual images (Fig. 12(b)(d)), only class 1 can be divided into two or three clusters roughly. The phenomenon of multiple clusters means that the flames generated by the same reactants condition have multiple significantly distinguishable modes/patterns. Corresponding to the image quality we discussed above, the cluster information tells that IR image has more diverse patterns inside the class, while visual image has more consistent patterns.

Benefited from the consistent patterns of visual images, the prototypes generated on visual images are far from each other, and inside the cluster of test samples (Fig. 12 (d)), so that PN can work almost perfectly on visual images. However, since the IR images are more elusive, PN cannot generate perfectly separated prototypes, instead, the prototypes of class 1, class 2, and class 5 are overlapped, as we point in Fig. 12 (c), which is why 46 images of class 1 (mentioned in Fig. 9 (c)) are misclassified as class 2. Since prototypes are not contrastive enough, the small cluster of class 5 neighboring a cluster of class 6 is misclassified to class 6, as the prototype of class 6 is closer to this small cluster. Meanwhile, from Fig. 12 (a), we also found that this small cluster has never been sampled to be part of training set, which in turn caused the generation of biased prototype. However, for SN-kNN, with the support from “worldwide” distribution of training set, it works much more robust on IR images.

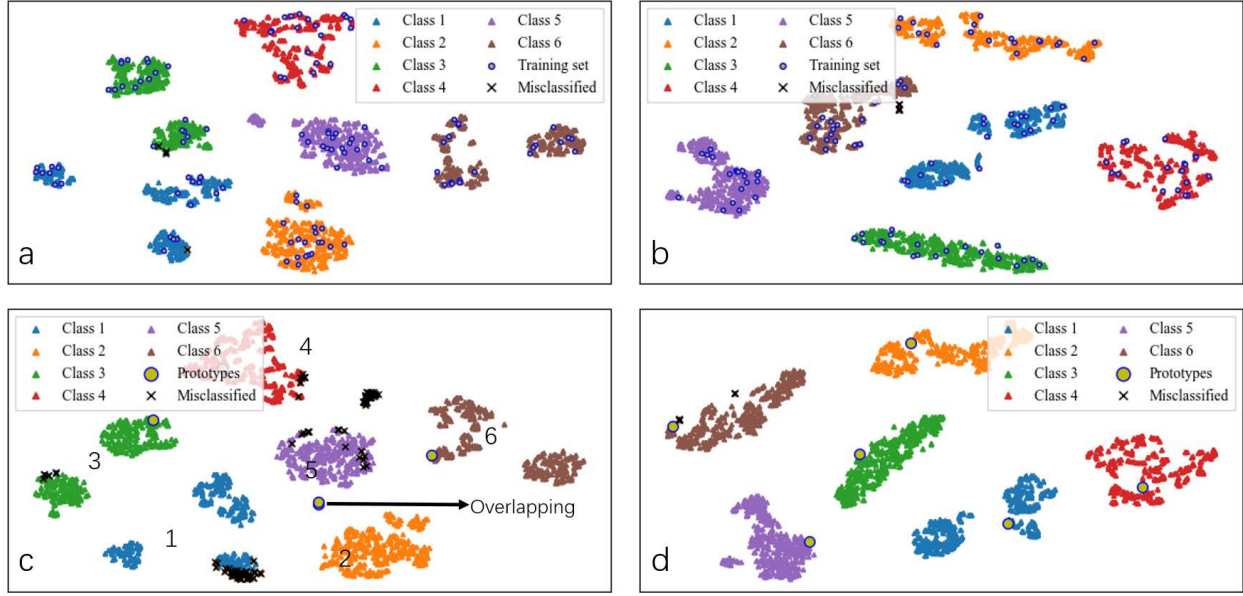


Figure 12: Visualization of features encoded by models (a) SN on IR images (b) SN on visual images (c) PN on IR images (d) PN on visual images

4 Conclusion

In this research, we developed two few-shot-learning-based combustion state monitoring algorithms, more specifically, learning to classify flame states from very few visual or IR images. From the results and analysis, we can conclude as follows:

1, Both algorithms, SN-kNN and PN, are capable to learn to classify flame states from only 20 visual or IR images per class and have decent performance in test. More specifically, the worst performance happened on PN on IR images, the Precision was 0.957, Accuracy, Recall, and F1-score was about 0.953. Through visualization of features, we found the reason is prototypical network are confused by IR images and cannot provide distinguishable prototypes for some classes, however, SN can utilize the regional distribution of training samples to support the flame state classifications, which is more robust.

2, Considering the task and algorithms here, visual image seems to be more suitable than IR images, since both models are easier to converge on visual images and the worst test performance happens on IR images. Through direct observation of images and visualization of learned features, we realize that the reason behind is visual images have more contrastive difference between flame states and also have more consistent patterns inside the class, this natural clustering property makes visual images easier to be classified.

3, PN only needed about 30 epochs to train, 47.4 ms to classify one IR image, 116.54 ms to classify one visual image. In contrast, SN-kNN needed much more time in training and inference, which is about 3.25 times, 28.66 times, and 19.75 times of PN, respectively. The advantages in preparation and inference time of PN, may be favoured by efficiency-dominating industrial applications.

References

- [1] Katharina Kohse-Höinghaus and Jay Barker Jeffries, editors. *Applied Combustion Diagnostics*. Combustion : An International Series. Taylor & Francis, New York, NY, 2002.
- [2] Ruiyuan Kang, Panos Liatsis, and Dimitrios C. Kyritsis. Emission Quantification via Passive Infrared Optical Gas Imaging: A Review. *Energies*, 15(9):3304, April 2022.
- [3] Xiaojing Bai, Gang Lu, Md Moinul Hossain, Yong Yan, and Shi Liu. Multimode Monitoring of Oxy-Gas Combustion Through Flame Imaging, Principal Component Analysis, and Kernel Support Vector Machine. *Combustion Science and Technology*, 189(5):776–792, May 2017.

- [4] Hao Zhou, Qi Tang, Linbin Yang, Yong Yan, Gang Lu, and Kefa Cen. Support vector machine based online coal identification through advanced flame monitoring. *Fuel*, 117(PARTB):944–951, 2014.
- [5] Zhezhe Han, Md Moinul Hossain, Yuwei Wang, Jian Li, and Chuanlong Xu. Combustion stability monitoring through flame imaging and stacked sparse autoencoder based deep neural network. *Applied Energy*, 259(August):114159–114159, 2020.
- [6] Julio Pino, Hugo O. Garcés, Juan Cuevas, Luis E. Arias, Alejandro J. Rojas, and Andrés Fuentes. Soot propensity by image magnification and artificial intelligence. *Fuel*, 225(March):256–265, 2018.
- [7] Yu Wang, Yuefeng Yu, Xiaolei Zhu, and Zhongxiao Zhang. Pattern recognition for measuring the flame stability of gas-fired combustion based on the image processing technology. *Fuel*, 270(August 2019):117486–117486, 2020.
- [8] Hua Chen, Tingting Yan, and Xiaogang Zhang. Burning condition recognition of rotary kiln based on spatiotemporal features of flame video. *Energy*, 211:118656–118656, 2020.
- [9] Danilo de Santana Chui, Flávio Trigo, Flavius Martins, and Agenor Fleury. Fuzzy inference of oil furnace combustion state through computer vision information. (March), 2019.
- [10] Weitao Li, Dianhui Wang, and Tianyou Chai. Flame image-based burning state recognition for sintering process of rotary kiln using heterogeneous features and fuzzy integral. *IEEE Transactions on Industrial Informatics*, 8(4):780–790, 2012.
- [11] Michael Hauser, Yue Li, Jihang Li, and Asok Ray. Real-time combustion state identification via image processing: A dynamic data-driven approach. *Proceedings of the American Control Conference*, 2016-July:3316–3321, 2016.
- [12] Danilo S. Chui, Gustavo C. Silva Neto, Flávio C. Trigo, Flavius P.R. Martins, and Agenor T. Fleury. On the dynamics of flame images identified through computer vision and modal methods. *Journal of the Brazilian Society of Mechanical Sciences and Engineering*, 42(6):1–15, 2020.
- [13] Junghui Chen, Tong Yang Hsu, Chih Chien Chen, and Yi Cheng Cheng. Monitoring combustion systems using HMM probabilistic reasoning in dynamic flame images. *Applied Energy*, 87(7):2169–2179, 2010.
- [14] Junghui Chen, Lester Lik Teck Chan, and Yi Cheng Cheng. Gaussian process regression based optimal design of combustion systems using flame images. *Applied Energy*, 111:153–160, 2013.
- [15] Duo Sun, Gang Lu, Hao Zhou, and Yong Yan. Condition monitoring of combustion processes through flame imaging and kernel principal component analysis. *Combustion Science and Technology*, 185(9):1400–1413, 2013.
- [16] MD Hossain. Combustion condition monitoring through deep learning networks. Elsevier, 2019.
- [17] Adedotun Akintayo, Kin Gwn Lore, Soumalya Sarkar, and Soumik Sarkar. Early Detection of Combustion Instabilities using Deep Convolutional Selective Autoencoders on Hi-speed Flame Video. 2016.
- [18] Tian Qiu, Minjian Liu, Guiping Zhou, Li Wang, and Kai Gao. An unsupervised classification method for flame image of pulverized coal combustion based on convolutional auto-encoder and hidden Markov model. *Energies*, 12(13), 2019.
- [19] Zhenyu Wang, Chunfeng Song, and Tao Chen. Deep learning based monitoring of furnace combustion state and measurement of heat release rate. *Energy*, 131:106–112, 2017.
- [20] Xiaobin Zhu, Zun Cai, Jianjun Wu, Yuqiang Cheng, and Qiang Huang. Convolutional neural network based combustion mode classification for condition monitoring in the supersonic combustor. *Acta Astronautica*, 159(April):349–357, 2019.
- [21] Tao Li, Zhenting Zhang, and Hua Chen. Predicting the combustion state of rotary kilns using a Convolutional Recurrent Neural Network. *Journal of Process Control*, 84:207–214, 2019.
- [22] Ouk Choi, Jongwun Choi, Namkeun Kim, and Min Chul Lee. Combustion instability monitoring through deep-learning-based classification of sequential high-speed flame images. *Electronics (Switzerland)*, 9(5), 2020.
- [23] Hervé Abdi and Lynne J. Williams. Principal component analysis. *Wiley Interdisciplinary Reviews: Computational Statistics*, 2(4):433–459, July 2010.
- [24] Bernhard Schölkopf, Alexander Smola, and Klaus-Robert Müller. Kernel principal component analysis. In *International Conference on Artificial Neural Networks*, pages 583–588. Springer, 1997.
- [25] T. Kohonen. The self-organizing map. *Proceedings of the IEEE*, 78(9):1464–1480, Sept./1990.
- [26] Ganggang Dong, Guisheng Liao, Hongwei Liu, and Gangyao Kuang. A review of the autoencoder and its variants: A comparative perspective from target recognition in synthetic-aperture radar images. *IEEE Geoscience and Remote Sensing Magazine*, 6(3):44–68, 2018.

- [27] Antonia Creswell, Tom White, Vincent Dumoulin, Kai Arulkumaran, Biswa Sengupta, and Anil A. Bharath. Generative Adversarial Networks: An Overview. *IEEE Signal Processing Magazine*, 35(1):53–65, January 2018.
- [28] William S Noble. What is a support vector machine? *Nature Biotechnology*, 24(12):1565–1567, December 2006.
- [29] M.W Gardner and S.R Dorling. Artificial neural networks (the multilayer perceptron)—a review of applications in the atmospheric sciences. *Atmospheric Environment*, 32(14-15):2627–2636, August 1998.
- [30] Christopher K Williams and Carl Edward Rasmussen. *Gaussian Processes for Machine Learning*, volume 2. MIT press Cambridge, MA, 2006.
- [31] Ahmed Ali Mohammed Al-Saffar, Hai Tao, and Mohammed Ahmed Talab. Review of deep convolution neural network in image classification. In *2017 International Conference on Radar, Antenna, Microwave, Electronics, and Telecommunications (ICRAMET)*, pages 26–31, Jakarta, October 2017. IEEE.
- [32] Ah Chung Tsoi. Recurrent neural network architectures: An overview. In Jaime G. Carbonell, Jörg Siekmann, G. Goos, J. Hartmanis, J. van Leeuwen, C. Lee Giles, and Marco Gori, editors, *Adaptive Processing of Sequences and Data Structures*, volume 1387, pages 1–26. Springer Berlin Heidelberg, Berlin, Heidelberg, 1998.
- [33] Abdul Rahman D Farraj, Ahmad M AL-Naeemy, Ashraf N Al-Khateeb, and Dimitrios C Kyritsis. Laminar non-premixed counterflow flames manipulation through the application of external direct current fields. *Journal of Energy Engineering*, 143(4):04017002, 2017.
- [34] Iaroslav Melekhov, Juho Kannala, and Esa Rahtu. Siamese network features for image matching. In *2016 23rd International Conference on Pattern Recognition (ICPR)*, pages 378–383, Cancun, December 2016. IEEE.
- [35] Liangxiao Jiang, Zhihua Cai, Dianhong Wang, and Siwei Jiang. Survey of Improving K-Nearest-Neighbor for Classification. In *Fourth International Conference on Fuzzy Systems and Knowledge Discovery (FSKD 2007)*, pages 679–683, Haikou, China, 2007. IEEE.
- [36] Jake Snell, Kevin Swersky, and Richard Zemel. Prototypical networks for few-shot learning. *Advances in neural information processing systems*, 30, 2017.
- [37] Karen Simonyan and Andrew Zisserman. Very Deep Convolutional Networks for Large-Scale Image Recognition, April 2015.
- [38] Kaiming He, Xiangyu Zhang, Shaoqing Ren, and Jian Sun. Deep residual learning for image recognition. In *Proceedings of the IEEE Conference on Computer Vision and Pattern Recognition*, pages 770–778, 2016.
- [39] Alexey Dosovitskiy, Lucas Beyer, Alexander Kolesnikov, Dirk Weissenborn, Xiaohua Zhai, Thomas Unterthiner, Mostafa Dehghani, Matthias Minderer, Georg Heigold, Sylvain Gelly, Jakob Uszkoreit, and Neil Houlsby. An Image is Worth 16x16 Words: Transformers for Image Recognition at Scale, June 2021.